ISSN No. 2454-6194 | DOI: 10.51584/IJRIAS | Volume VIII Issue IV April 2023

Mathematical Model and Simulation of Blood Flow Dynamics in Renal Interlobar Artery of Patients with Human immunodeficiency Virus

Abubakar, U.[1], Ugwu, A. C.[2], Tivde, T.[3] and Mbah, GCE[4]

[1]Department of Radiography, Usmanu Danfodiyo University, Sokoto, Nigeria
[2]Department of Radiography and Radiological Sciences, Nnamdi Adzikiwe University, Awka, Nigeria
[3]Department of Mathematics, Joseph Sarwuan Tarka University, Makurdi, Nigeria
[4]Department of Mathematics, University of Nigeria, Nsukka, Nigeria

DOI: https://doi.org/10.51584/IJRIAS.2023.8405

Received: 28 October 2022; Accepted: 17 November 2022; Published: 28 April 2023

Abstract: Mathematical models were developed considering wall movement, blood pulsation and flow dynamics of the blood in the interlobar artery. The formulated models were based on the fact that the motion of blood vessel wall is not only influenced by pulsation, but also other physiological processes like heartbeat, breathing, and body posture. The Newton's second Law of motion was employed in assembling the forces acting on the interlobar artery. The wall shear stress (WSS) was studied alongside, arterial walls to study the actual flow dynamics and investigate the blood flow behaviour. The results of the study were presented on both two – dimensional (2D) and three (3D) – dimensional graphs showing a more realistic interaction between the arterial wall and the blood flow in patients with HIV/AIDS. It was deduced that the blood flow velocity decreased with time across the varying frequency from 0.20Hz to 0.50Hz in the interlobar arterial channel.

Keywords: *Mathematical Modelling, Blood flow, interlobar artery, blood flow dynamics, blood flow velocity, wall shear stress*

Reference to this paper should be made as follows:

Biographical notes: (ABS)

I. Introduction

Human Immunodeficiency Virus (HIV) is an infection that attacks the body's immune system and over time, if not treated, leads to acquired immunodeficiency syndrome (AIDS)[1]. Human Immunodeficiency Virus Associated Nephropathy (HIVAN) is the commonest cause of renal failure in HIV- 1- seropositive patients and the third most common end stage renal failure in African Americans between the ages of 20 to 64 [2]. Various types of renal disease were identified in the AIDS populace including those related to systemic and local renal infections, tubule interstitial disease, renal associated neoplasm and glomerular infection including collapsing glomerulopathy[3]. Atherosclerosis causes stenosis in the artery and is one of the most common types of cardiovascular disease.

The main cause of stenosis is the formation of plaque by the accumulation of cholesterol, lipid substances, cellular waste products, calcium, and fibrin in the endothelium of the tunica intima. The plaque may lead to stenosis or atresia in the artery, which may eventually result to heart attack and stroke [4]-[6]. Additionally, it is a proven fact that once a mild stenosis is developed, it will result to flow disorders that will consequently change the regional blood rheology, arterial deformability and influence the development of the disease[7].

Consequently, many scientific researchers have made remarkable efforts to develop new velocimetry estimation, signal processing, clutter filter, and visualization techniques to obtain more accurate signals of blood flow [16]. It is imperative to evaluate these new techniques. In order to overcome the aforementioned challenges faced by diagnostic ultrasound, the computer simulation is a useful validation method because all parameters can be well defined. Hence, some researchers developed mathematical models and simulations to imitate the behaviour of pulsatile blood flow based on the assumption that the wall of the artery is rigid[17-19]. Recently, taking into cognizance the compromised SNR as a result of interaction between blood flow and the vessel wall, several researchers have developed more realistic and complex models with the aid of computational fluid dynamics (CFD) software[20-26].

The Renal Arteries Arise from the Abdominal Aorta. The single renal artery enters the hilum and then branches to form the *interlobar arteries*, so-named because they pass between the lobes of the kidney. At the junction of the cortex and medulla, the interlobar arteries bend over to form incomplete arches.

ISSN No. 2454-6194 | DOI: 10.51584/IJRIAS | Volume VIII Issue IV April 2023

In this study, mathematical models were developed considering wall movement, blood pulsation and flow dynamics of the blood. The motion of blood vessel wall is not only influenced by pulsation, but also other physiological processes such as heartbeat, breathing, and body posture[27,28]. This coupled method provides a better understanding of the relationship between ultrasound images and the actual flow dynamics, as well as a better investigation of blood flow behaviour. The objective of this study is to develop a mathematical model and simulations that can generate more realistic ultrasound echoed signals, considering the interaction between the arterial wall and the blood flow in patients with HIV/AIDS. The developed model and simulation would also serve as a useful tool for investigating the behaviour of renal interlobar arterial flow dynamics but also for qualitative or quantitative evaluation of new Doppler or greyscale ultrasound imaging technology and the estimation of blood velocimetry.

II. Model Formulation

The mathematical model governing the flow of blood in the interlobar artery is formulated following the procedure: Assumptions of the model, model parameters/variables, model flow diagram (geometric deformation of the interlobar artery) and hence, the governing equation.

2.1 Assumptions of the model

The model is formulated based on the following assumptions:

a. The total momentum of interlobar blood flow system is preserved in lack of external forces acting on the blood element.
b. The tapering of the arterial wall radius at the axial and distance increases away from the lobar artery.
c. Blood is considered as an ideal Newtonian fluid with constant viscosity, whereas the flow is steady and laminar, with a parabolic flow profile.
d. Shear forces exist between adjacent flow laminar, as well as the outermost laminar, and on the wall of the interlobar artery.
e. Interlobar arterial wall movement, blood pulsation and flow dynamics of the blood in the interlobar artery.
f. The interlobar artery is distensible
g. The motion of blood flow in the model is viewed in both radial and axial directions
h. The pressure gradient in the outer wall is greater than the pressure in the inner walls of the interlobar artery.
i. The blood flowing in the interlobar artery is incompressible with its motion being laminar and steady

2.2 Model parameters and variables

The variables of the model are presented in *Table 1*.

Table 1 Model variables and their meanings

S/N	Variable	Meaning
(i)	r	Distensible radius of the interlobar artery at time, t
(ii)	z	Location in the interlobar arterial region
(iii)	t	Time of flow of blood
(iv)	u	Velocity of blood in the axial direction
(v)	v	Velocity of blood in the radial direction

2.3. Model parameters

The variables of the model are presented in Table 2.

ISSN No. 2454-6194 | DOI: 10.51584/IJRIAS | Volume VIII Issue IV April 2023

Table 1 Model parameters and their meanings

S/N	Variable	Meaning
1	θ	Angle of tapering
2	φ	Amplitude ratio for the distensible wall of the interlobar artery
3	λ	Wavelength
4	ξ	Amplitude ratio for the distensible wall of the interlobar artery
5	R_0	Undisturbed radius of the distensible interlobar artery
6	r	Radius of the interlobar artery at time, t
7	z	Location in the interlobar arterial region
8	ω	Angular interlobar blood flow velocity
9		

2.4 Model Flow Diagram

The interlobar arteries are vessels of the renal circulation which supply the renal lobes are presented here showing clearly that interlobar arteries branch from the lobar arteries which branch from the segmental arteries, from the renal artery thereby giving rise to arcuate arteries.

A schematic diagram showing a truncation of geometry of the interlobar artery is presented in Figure 2a and 2b which is the model flow diagram for the system.

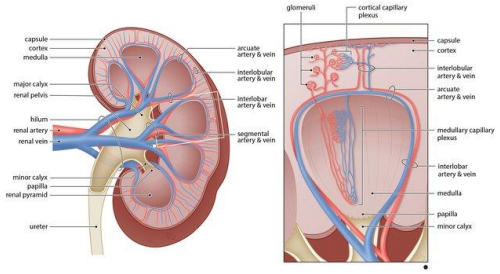

Figure 1: Anatomy of the renal vasculature [34]

Blood enters the kidney via the renal artery which divides dichotomously into segmental arteries and branch progressively into *interlobar arteries.* Arcuate arteries, separating the border between the cortex and medulla, giving rise to interlobular arteries which further diverge to supply the glomeruli. Besides the glomerular capillary network, the renal microcirculation can be divided into cortical and medullary capillary plexus based on the anatomical location. Finally, blood flows via the arcuate, interlobar, and segmental veins to exit the kidney via the renal vein [34].

A schematic diagram showing this flow process in the interlobar artery is as shown in *Figure 2a* and *Figure 2b.*

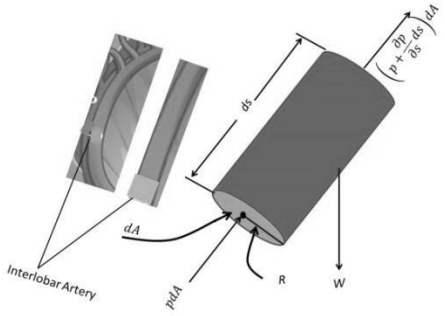

Figure 2a: Schematic diagram showing the flow process in the interlobar artery

ISSN No. 2454-6194 | DOI: 10.51584/IJRIAS | Volume VIII Issue IV April 2023

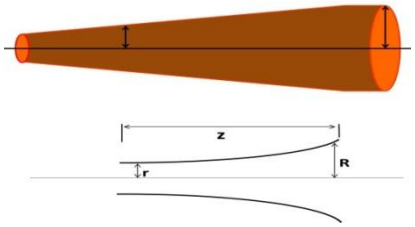

Figure 2b: Schematic diagram showing the flow process in the interlobar artery (tapered in shape)

Analyzing the tapering, the radius of the interlobar artery is given by;

$$r = R_0 - ztan\theta \quad (1)$$

And considering an interlobar artery with a stenotic growth in the inner walls of the artery to a height of δ, then the radius is given by equation (1);

$$R = r\left[1 \pm \delta sin\frac{2\pi}{\lambda}(z - ct)\right] \quad (2)$$

2.5 The Governing Equation

The governing equation is the mathematical model of blood flow in the interlobar artery which is formulated based on the law of conservation of mass. As per this principle, total momentum of every fluid system is preserved in lack of outside force. So the law of conservation of momentum is appropriate to renal circulatory system and applied specifically to the interlobar artery.

In addition, rate of change of momentum of a fluid particle with respect to time equals to external force exerted on it, which is also known as Newton's second law of motion [36]. Therefore, rate of change of momentum is same as sum of regarding two mentioned forces, which could be symbolically presented following Newton's Law:

$$F = ma \quad (3)$$

Where F is force acting on the blood element, m is mass

and a is the acceleration of the blood element. Knowing fully well that acceleration, $a = \frac{dv}{dt}$ and velocity of blood, $= \frac{ds}{dt}$, we write

$$F = m\frac{dv}{dt} = m\frac{d^2s}{dt} = \frac{m}{ds}.\frac{d^2s}{dt^2}ds$$

$$F = \frac{m}{\Delta V}.\Delta V.a_s = \rho dsdAa_s = \rho gdAds$$

Where $density\ of\ blood,\ \rho = \frac{m}{\Delta V}$, ΔV being change in volume of blood in the interlobar artery with cross-sectional area, dA and we have;

$$F = \rho gdsdA \quad (4)$$

Considering *Figure 2a***,** the summation of all the infinitesimal forces acting on the blood element in the interlobar artery is deduced to be:

$$F_i = pdA - \left(p + \frac{\partial p}{\partial s}ds\right)dA - \rho gdsdAcos\theta \quad (5)$$

Equating (4) and (5) we have

$$\Rightarrow pdA - \left(p + \frac{\partial p}{\partial s}ds\right)dA - \rho gdsdAcos\theta = \rho gdsdA = \rho dAdsa_s$$

where $a = a_x + a_y + a_z$, with

ISSN No. 2454-6194 | DOI: 10.51584/IJRIAS | Volume VIII Issue IV April 2023

$$\left.\begin{aligned} a_x &= u\frac{\partial u}{\partial x} + v\frac{\partial u}{\partial y} + w\frac{\partial u}{\partial t} + \frac{\partial u}{\partial t} \\ a_y &= u\frac{\partial v}{\partial x} + v\frac{\partial v}{\partial y} + w\frac{\partial v}{\partial t} + \frac{\partial v}{\partial t} \\ a_z &= u\frac{\partial w}{\partial x} + v\frac{\partial w}{\partial y} + w\frac{\partial w}{\partial t} + \frac{\partial w}{\partial t} \end{aligned}\right\} \quad (6)$$

As such, we have in rectangular, cylindrical, and spherical coordinate systems as preserved by equations (6a), (6b) and (6c) respectively;

$$\frac{\Delta}{\Delta t} = u\frac{\partial}{\partial x} + v\frac{\partial}{\partial y} + w\frac{\partial}{\partial z} + \frac{\partial}{\partial t} \quad (6a)$$

$$\frac{\Delta}{\Delta t} = v_r\frac{\partial}{\partial r} + \frac{v_\theta}{r}\frac{\partial}{\partial \theta} + v_z\frac{\partial}{\partial z} + \frac{\partial}{\partial t} \quad (6b)$$

and

$$\frac{\Delta}{\Delta t} = v_r\frac{\partial}{\partial r} + \frac{v_\theta}{r}\frac{\partial}{\partial \theta} + \frac{v\phi}{rsin\theta}\frac{\partial}{\partial z} + \frac{\partial}{\partial t} \quad (6c)$$

Such that, acceleration in cylindrical coordinates is given by

$$\left.\begin{aligned} a_r &= v_r\frac{\partial v_r}{\partial r} + \frac{v_\theta}{r}\frac{\partial v_r}{\partial \theta} + v_z\frac{\partial v_r}{\partial z} - \frac{v^2\theta}{r} + \frac{\partial v_r}{\partial t} \\ a_\theta &= v_r\frac{\partial v_\theta}{\partial r} + \frac{v_\theta}{r}\frac{\partial v_\theta}{\partial \theta} + v_z\frac{\partial v_\theta}{\partial z} - \frac{v^2\theta}{r} + \frac{\partial v_\theta}{\partial t} \\ a_z &= v_r\frac{\partial v_z}{\partial r} + \frac{v_\theta}{r}\frac{\partial v_z}{\partial \theta} + v_z\frac{\partial v_z}{\partial z} + \frac{\imath}{r} \cdot \frac{\partial v_z}{\partial t} \end{aligned}\right\} \quad (7)$$

$$\rho\frac{\partial U}{\partial T} = -\frac{\partial P}{\partial R} + \mu\left[\frac{\partial^2 U}{\partial R^2} + \frac{1}{R}\frac{\partial U}{\partial R} - \frac{U}{R^2} + \frac{\partial^2 U}{\partial Z^2}\right]$$

Let $= v = \frac{V}{v_0},\ u = \frac{U}{u_0},\ p = \frac{P}{\rho V_0^2},\ t = \frac{T\,v_0}{R_0},\ z = \frac{Z}{z_0},\ r = \frac{R}{R_0},\ with\ z_0 = R_0$

$\Rightarrow V = vv_0,\ U = uu_0,\ P = \rho V_0^2 P,\ T = \frac{tR_0}{V_0},\ Z = zz_0,\ R = R_0 r$

$Z_0 \approx R_0$

Also $\rho = \frac{P}{Pv_0^2} = \frac{\rho v_0^2 P}{Pv_0^2}$

$\Rightarrow \rho = \rho = 1$

Thus substituting we have;

$$\Rightarrow \frac{\partial uu_0}{\frac{\partial tR_0}{v_0}} = -\frac{\partial v_0^2 P}{\partial rR_0} + \mu\left[\frac{\partial^2 uu_0}{\partial R_0^2 r^2} + \frac{1}{R_0 r}\frac{\partial uu_0}{\partial R_0 r} - \frac{uu_0}{R_0^2 r^2} + \frac{\partial^2 u^2 u_0}{\partial z^2 z_0^2}\right]$$

$$\Rightarrow \frac{\partial u}{\partial t}\left(\frac{u_0 v_0}{R_0}\right) = -\frac{\partial P v_0^2}{\partial rR_0} + \mu\left[\frac{\partial^2 uu_0}{\partial r^2 R_0^2} + \frac{1}{R_0 r}\frac{\partial uu_0}{\partial rR_0} - \frac{uu_0}{R_0^2 r^2} + \frac{\partial^2 uu_0}{\partial z^2 z_0^2}\right]$$

$$\Rightarrow \frac{\partial u}{\partial t} = \frac{\partial p v_0^2 R_0}{\partial rR_0 u_0 v_0} + \mu\left[\frac{\partial^2 uu_0 R_0}{\partial r^2 R_0^2 u_0 v_0} + \frac{1}{R_0 r}\frac{\partial uu_0 R_0}{\partial rR_0 u_0 v_0} - \frac{uu_0 R_0}{R_0^2 r^2 u_0 v_0} + \frac{\partial^2 uu_0 R_0}{\partial z^2 R_0^2 u_0 v_0}\right]$$

$$\frac{\partial u}{\partial t} = \frac{\partial p}{\partial r}\left(\frac{v_0}{u_0}\right) + \mu\left[\frac{\partial^2 u}{\partial r^2}\left(\frac{1}{R_0 v_0}\right) + \frac{\partial u}{r\partial r}\left(\frac{1}{R_0 v_0}\right) - \frac{u}{r^2}\left(\frac{1}{R_0 v_0}\right) + \frac{\partial^2 u}{\partial z^2}\left(\frac{1}{R_0 v_0}\right)\right]$$

But $\frac{v_0}{u_0} = 1\ since\ v_0 = \frac{V}{v} = \frac{vv_0}{v} \Rightarrow\ v_0 = v_0 = 1$

$similarly\ u_0 = 1, hence$

ISSN No. 2454-6194 | DOI: 10.51584/IJRIAS | Volume VIII Issue IV April 2023

$$\frac{\partial u}{\partial t} = \frac{\partial p}{\partial r} + \frac{\mu}{R_0 v_0}\left[\frac{\partial^2 u}{\partial r^2} + \frac{\partial u}{r\partial r} - \frac{u}{r^2} + \frac{\partial^2 u}{\partial z^2}\right]$$

let $\frac{\mu}{R_0 v_0} = \frac{1}{R_e}$

$$\therefore \frac{\partial u}{\partial t} = \frac{\partial p}{\partial r} + \frac{1}{R_e}\left[\frac{\partial^2 u}{\partial r^2} + \frac{\partial u}{r\partial r} - \frac{u}{r^2} + \frac{\partial^2 u}{\partial z^2}\right] \qquad (8)$$

Similarly, considering equation (8) we set the dimensionless quantities as follows;

Let $V = vv_0, P = \rho v_0^2 p,\ T = \frac{tR_0}{v_0},\ \ Z = zz_0\ ,\ R = R_0 r,\ z_0 = R_0$, taking $\rho = 1,\ v_0 = 1$

with $z_0 = 1$ and substituting into equation (3.9) we have;

$$\frac{\frac{\partial vv_0}{\partial tR_0}}{v_0} = -\frac{\partial \rho v_0^2 p}{\partial z z_0} + \mu\left[\frac{\partial^2 vv_0}{\partial R_0^2 r^2} + \frac{1}{r}\frac{\partial vv_0}{\partial R_0 r} + \frac{\partial^2 vv_0}{\partial z^2 z_0^2}\right]$$

$$\frac{\partial v}{\partial t}\left(\frac{v_0 v_0}{tR_0}\right) = -\frac{\partial \rho v_0^2}{\partial z R_0} + \mu\left[\frac{\partial^2 vv_0}{\partial R_0^2 r^2} + \frac{1}{r}\frac{\partial vv_0}{\partial r R_0} + \frac{\partial^2 vv_0}{\partial z^2 R_0^2}\right]$$

$$\frac{\partial v}{\partial t} = -\frac{\partial \rho v_0^2}{\partial z v_0^2 R_0} + \mu\left[\frac{\partial^2 vv_0 R_0}{\partial r^2 v_0^2 R_0^2} + \frac{1}{r}\frac{\partial vv_0 R_0}{\partial r v_0^2 R_0} + \frac{\partial^2 vv_0 R_0}{\partial z^2 R_0^2 v_0^2}\right]$$

$$\frac{\partial v}{\partial t} = -\frac{\partial \rho}{\partial z} + \mu\left[\frac{\partial^2 v}{\partial r^2}\frac{1}{v_0 R_0} + \frac{\partial v}{r\partial r}\frac{1}{v_0 R_0} + \frac{\partial^2 v}{\partial z^2 v_0 R_0}\right]$$

$$\frac{\partial v}{\partial t} = -\frac{\partial \rho}{\partial z} + \frac{\mu}{v_0 R_0}\left[\frac{\partial^2 v}{\partial r^2} + \frac{\partial v}{r\partial r} + \frac{\partial^2 v}{\partial z^2}\right]$$

Considering, $\frac{\mu}{v_0 R_0} = \frac{1}{R_e}$, we have

$$\frac{\partial v}{\partial t} = -\frac{\partial \rho}{\partial z} + \frac{1}{R_e}\left[\frac{\partial^2 v}{\partial r^2} + \frac{\partial v}{r\partial r} + \frac{\partial^2 v}{\partial z^2}\right]. \qquad (9)$$

In summary, the governing model for the system is given by equation (10)

$$\left.\begin{aligned} \frac{\partial u}{\partial t} &= \frac{\partial p}{\partial r} + \frac{v_0 R_0}{\mu}\left[\frac{\partial^2 u}{\partial r^2} + \frac{\partial u}{r\partial r} - \frac{u}{r^2} + \frac{\partial^2 u}{\partial z^2}\right] \\ \frac{\partial v}{\partial t} &= -\frac{\partial p}{\partial z} + \frac{v_0 R_0}{\mu}\left[\frac{\partial^2 v}{\partial r^2} + \frac{\partial v}{r\partial r} + \frac{\partial^2 v}{\partial z^2}\right] \\ \frac{1}{r}\frac{\partial}{\partial r}[ru(t,r,z)] &+ \frac{\partial v}{\partial z} = 0 \end{aligned}\right\} \qquad (10)$$

2.6 Solution of the model

The solution of the model is obtained using Bessel equations. Taking the fact that the arterial wall is elastic, then u, v and p are all functions of r, z, t so that introducing the boundary conditions;

$$u = 0, r = a\ (maximum), \frac{\partial v}{\partial r} = 0, r = 0$$

$$u(r,z,t) = v_1(r)e^{[i(n\omega t - y_n z)]} \qquad (11)$$

$$v(r,z,t) = v_2(r)e^{[i(n\omega t - y_n z)]} \qquad (12)$$

$$p(r,z,t) = p_1(r)e^{[i(n\omega t - y_n z)]} \qquad (13)$$

Substituting equations (11), (12) and (13) in equations (10) we obtain the second order ordinary differential equations for which the solutions are obtained as the Bessel's functions in terms of $J_0(iy_n r),\ J_0(ik_n r), J_1(iy_n r)\ and\ J_1(ik_n r)$. The solutions for$u(r,z,t)$, $v(r,z,t)$ and $p(r,z,t)$ have been obtained as shown in equations (14), (15) and (16) respectively;

$$u(r,z,t) = \left[\alpha y_n J_1(iy_n r) + \beta y_n J_1\left(ir\sqrt{y_n^2 + in\omega R_e}\right)\right]e^{i(n\omega t - y_n z)} \qquad (14)$$

ISSN No. 2454-6194 | DOI: 10.51584/IJRIAS | Volume VIII Issue IV April 2023

$$v(r,z,t) = \left[\alpha y_n J_0(iy_n r) + \beta y_n J_1\left(ir\sqrt{y_n^2 + in\omega R_e}\right)\right] e^{i(n\omega t - y_n z)} \quad (15)$$

$$p(r,z,t) = \alpha n\omega J_0(iy_n r) e^{i(n\omega t - y_n z)} \quad (16)$$

So that the velocity, $v(r,z,t)$ of blood flow in the interlobar artery is obtained as in equation (17)

$$v(r,z,t) = \begin{cases} 1.25e^{0.06061t}\left[\alpha\begin{pmatrix}0.907143\\ +\,0.091429\mathrm{R}^2 + \cdots\end{pmatrix} + \beta\begin{pmatrix}80.071486\\ +\,6348.6857\mathrm{R}^2 + \cdots\end{pmatrix}\right]\cos(\omega t - 0.6352) \\ 1.25e^{-0.0476t}\left[\alpha\begin{pmatrix}0.907143\\ +\,0.091429\mathrm{R}^2 + \cdots\end{pmatrix} + \beta\begin{pmatrix}80.071486\\ +\,6348.6857\mathrm{R}^2 + \cdots\end{pmatrix}\right]\cos(\omega t - 0.6352 \end{cases} \quad (17))$$

Pressure in the interlobar artery is determined as;

$$P(r,z,t) = \begin{cases} \frac{1.25\omega}{R}e^{0.06061t}\left[\alpha\begin{pmatrix}0.907143\\ +\,0.091429\mathrm{R}^2 + \cdots\end{pmatrix} + \beta\begin{pmatrix}80.071486\\ +\,6348.6857\mathrm{R}^2 + \cdots\end{pmatrix}\right]\cos(\omega t - 0.6352) \\ \frac{1.25\omega}{R}e^{-0.0476t}\left[\alpha\begin{pmatrix}0.907143\\ +\,0.091429\mathrm{R}^2 + \cdots\end{pmatrix} + \beta\begin{pmatrix}80.071486\\ +\,6348.6857\mathrm{R}^2 + \cdots\end{pmatrix}\right]\cos(\omega t - 0.6352) \end{cases}$$

III. Results and Discussion

The result of the study is presented in Figures 3 - 11, taking key from the variables and parameter values from Table 2.

Table 3: Values of the model flow

S/N	Variable	Values	Source
1	θ	$0^0\ to\ 60^0$	Gao *et al.*(2011)
2	δ	$1.5 \times 10^{-5}m$	Chakrabarty (2000)
3	λ	9.90mm	Tang (2002)
4	ξ	0.08	Tang (2002)
5	R_0	$3.50 \times 10^{-5}m$	Tang (2002)
6	r	$3.50 \times 10^{-5}m$	Tang (2002)
7	z	$0.008\ to\ 0.010m$	Manjunatha (2015)
8	f	0.0Hz to 0.60Hz	Gao *et al.*(2011)
8	ω	2πf	Gao *et al.*(2011)
9	α	0.5	Assumed
10	β	0.5	Assumed

ISSN No. 2454-6194 | DOI: 10.51584/IJRIAS | Volume VIII Issue IV April 2023

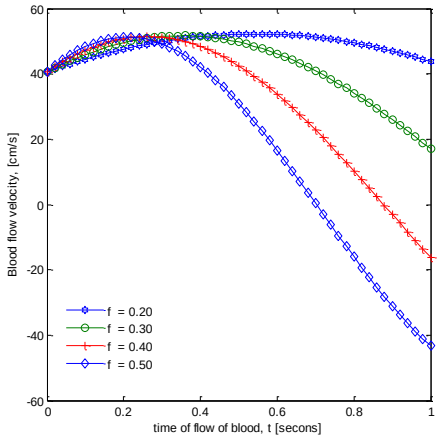

Figure 3: Graph of blood flow velocity within one second of time at a varying frequency from 0.20 Hz to 0.50 Hz in the interlobar artery

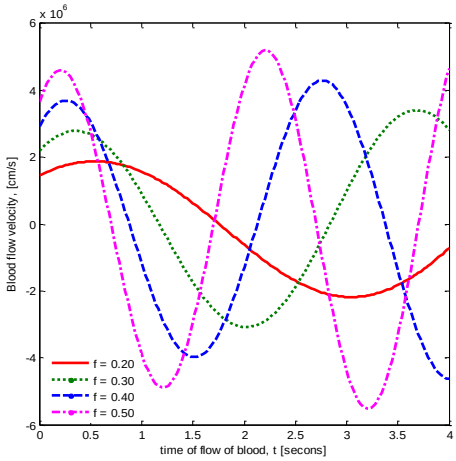

Figure 4: Graph of blood flow velocity within the first four units of time at a varying frequency in the interlobar artery from 0.20Hz to 0.50Hz in the interlobar artery

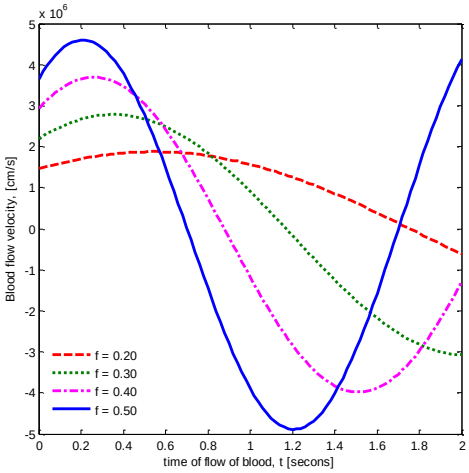

Figure 5: Graph of blood flow velocity 2 seconds of time at a varying frequency in the interlobar artery from 0.20Hz to 0.50Hz in the interlobar artery.

ISSN No. 2454-6194 | DOI: 10.51584/IJRIAS | Volume VIII Issue IV April 2023

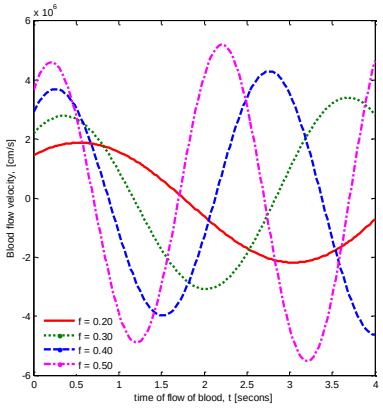

Figure 6: Graph of blood flow velocity within the first four units of time at a varying frequency in the interlobar artery from 0.20Hz to 0.50Hz in the interlobar artery

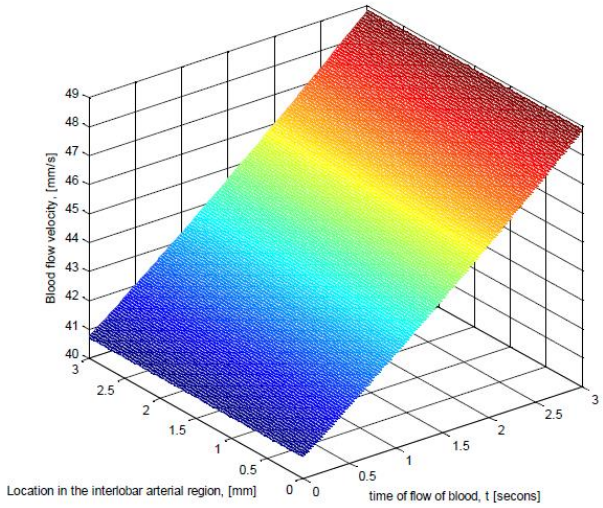

Figure 7: A 3D graph showing blood flow velocity in a region, 0 mm to 3mm of the interlobar artery within the 3 units of time at a frequency 0.20Hz

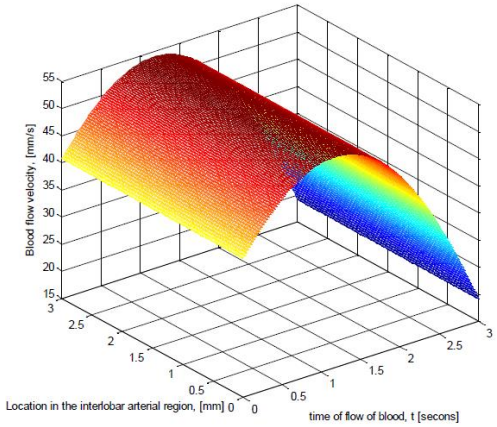

Figure 8: A 3D graph showing blood flow velocity in a region, 0 mm to 3mm of the interlobar artery within the 3 units of time at a frequency 0.30Hz

ISSN No. 2454-6194 | DOI: 10.51584/IJRIAS | Volume VIII Issue IV April 2023

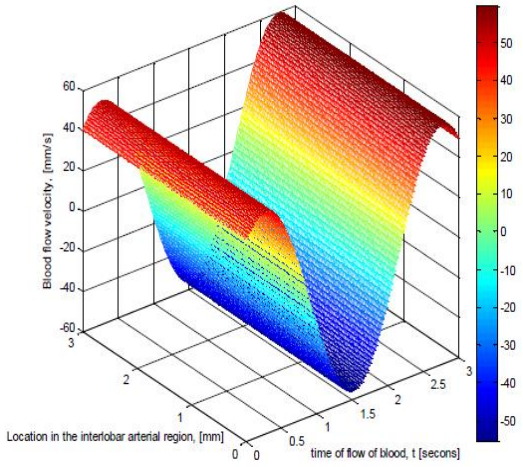

Figure 8a

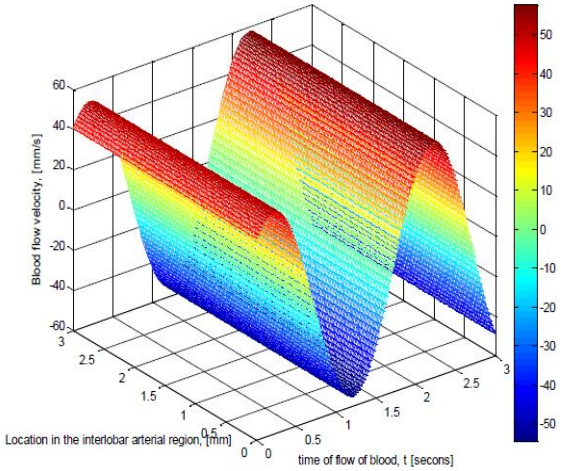

Figure 8b

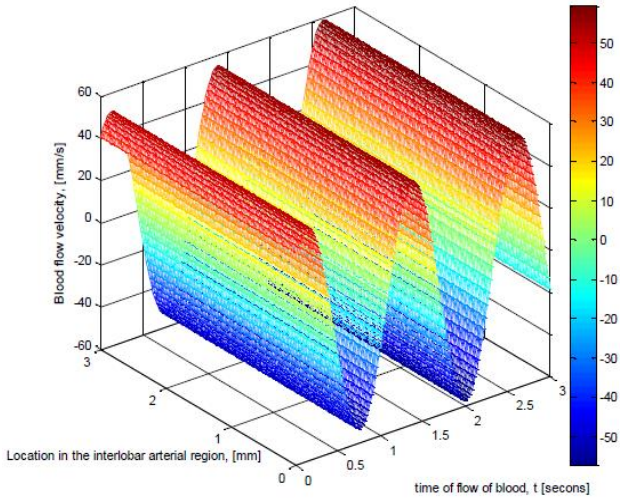

Figure 8c

ISSN No. 2454-6194 | DOI: 10.51584/IJRIAS | Volume VIII Issue IV April 2023

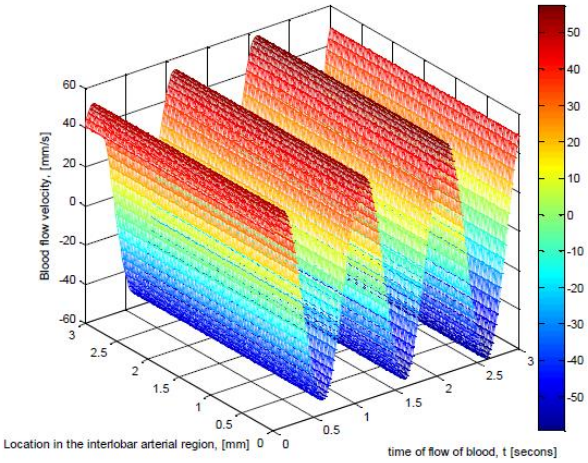

Figure 8d

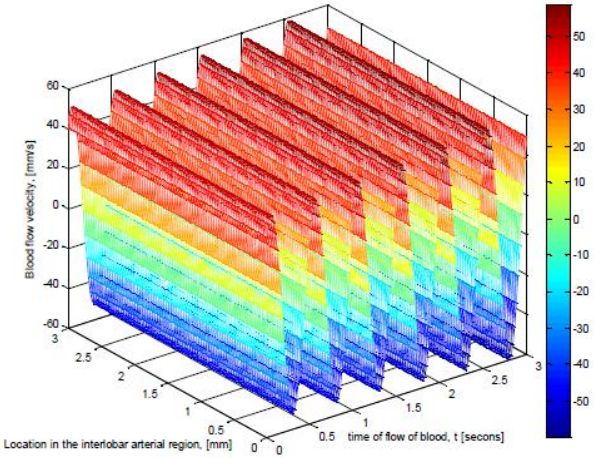

Figure 8e

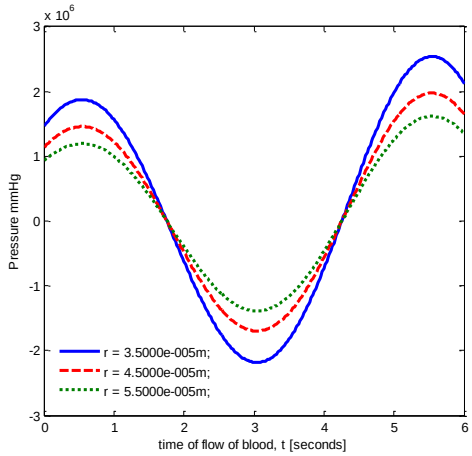

Figure 9: Graph of pressure generated across a tapered interlobar arterial channel

ISSN No. 2454-6194 | DOI: 10.51584/IJRIAS | Volume VIII Issue IV April 2023

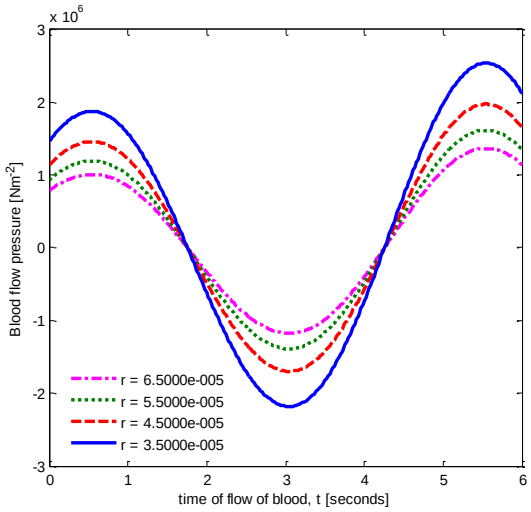

Figure 10: Blood flow pressure in a tapered artery with a varying radius from 3.5 x 10^{-5}m to 6.5 x 10^{-5}m studied within six seconds.

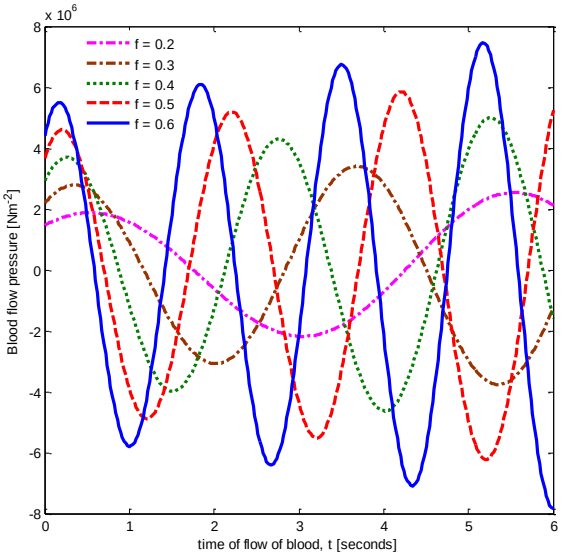

Figure 11: Blood flow pressure in a tapered artery with a varying radius from 3.5 x 10^{-5}m to 6.5 x 10^{-5}m studied within six seconds across different flow frequencies ranging from 0.2Hz to 0.6Hz

IV. Discussion

It is shown on Figure 3 that blood flow velocity in the interlobar artery increased from 40 cm/s to a peak of 50 cm/s in the first 0.2 seconds at a varying frequency of 0.20 Hz to 0.50 Hz then decreased as the frequency of flow increased across the arterial channel. This trend is clearly seen by increasing time of flow to 2 seconds and finally to 4seconds as shown in Figures 4 and 5. It is clearly shown that the velocity continued to move in a wavelike pattern due to pulsatility nature of blood flow in the artery.

Figures 3 – 6 is used in post processing to obtain the time averaged maximal velocity (TAVmax) and time averaged intensity weighted mean velocity (TAVmean). In Figure 5 and 6, the TAVmax was calculated by adding the area under the curve for positive velocities and the area above the curve for negative velocities and then dividing by the R-R interval. This second retrograde flow was included when calculating the TAV during diastole and during the entire cardiac cycle. During hyperemia, the flow velocities increased, and the waveform changed from triphasic to monophasic with continuous anterograde flow due to the pressure gradient created as a result of tissue ischemia, capillary dilatation, and decreased peripheral resistance as shown in Figure 7 and 8.

ISSN No. 2454-6194 | DOI: 10.51584/IJRIAS | Volume VIII Issue IV April 2023

Figures 8a – 8d are the three-dimensional plots showing the variation in the flow velocity across the cross-sectional area of the interlobar artery. The figures confirm the pattern of flow velocity shown in Figures 3 – 7.

It was further observed from Figure 9 that blood flow pressure decreases with an increasing radius of the artery in a wavelike pattern. This trend could only be observed from the recoil of blood flow (back flow) being in consonance with [38]. Hence, the blood flow within the interlobar artery depends on the pumping action of the heart, the elastic recoil of the conduit arteries, and distal microvasculature resistance. Thus, blood flow is quantified as a product of the mean blood velocity and the area across the interlobar artery thereby confirming [37]

This becomes so clear that in the resting state, the arteries displayed a triphasic waveform as such, interlobar arterial flow demonstrated forward flow that occurred during systole, whereas retrograde flow followed by anterograde flow occurred at diastole. There was an intervening pause with little to no flow before the next waveform (Figure 10).

It could be inferred that retrograde flow occurred again after the anterograde diastolic flow, giving a quadriphasic waveform that may be seen in lower extremity of interlobar arteries at rest as shown in Figure 10.

Again, the converse of the trend presented in Figure 9 is found in Figure 10 showing that the pressure increased with a decrease in the cross sectional area of the artery in the first one second and decreased by forming a parabolic surface.

It is deduced from Figure 11 that the pressure of flow is minimum at f = 0.20Hz and tends to vary in a wavelike style and becoming more turbulent at the arterial walls as the frequency increased from 0.30Hz to 0.60Hz which would continue to increase the quantity of flow of blood at a constant length and viscosity as the radius or velocity increases.

V. Conclusion

In conclusion, the formulated model was used in studying the velocity and pressure of flow of blood in the interlobar artery. The study of used data from HIV patients revealing that at different hemodynamic states, the velocity profile of blood flowing in the interlobar artery may not have a fully formed parabolic shape yielding some degree of bluntness of the velocity profile. Subsequent works may need to consider this and be measured during flow studies and incorporated into calculations for shear rate and blood flow.

References

1. Sidi, M., Ugwu, A. C., England, A., Manafa, P. O., Dambatta, A. H., Zira, J. D., … Mansur, U. Renal Doppler indices and their correlation with laboratory indices of human immunodeficiency virus seropositive adult individuals. *Radiography*, 2021; 27(4):1014-1020.
2. Barisoni, L., Bruggeman, L, A., Mundel, P., D'Agati, V, D., and Klotman, P, E. HIV- 1 induces renal epithelial dedifferentiation in a transgenic model of HIV- associated nephropathy. *Kidney International* 2000; 58:173-181.
3. Avila- Casado, M, C., Fortoul T, I., Chugh S, S. HIV- Associated Nephropathy: Experimental Models. *Contributions to Nephrology* 2011; 169: 270-285.
4. Texon, M. A hemodynamic concept of atherosclerosis, with particular reference to coronary occlusion. *AMA Archives of Internal Medicine* 1997; 99 (3): 418-427.
5. Caro, C. G., Fitz-Gerald J. M., and Schroter, R. C. Atheroma and arterial wall shear observation, correlation and proposal of a shear dependent mass transfer mechanism for atherogenesis. Proceedings of the Royal Society of London, Series B, *Biological sciences* 1971; 177(46): 109-159.
6. Fry, D. L. Acute vascular endothelial changes associated with increased blood velocity gradients. *Circulation Research* 1968; 22(2): 165–197.
7. Liepsch, D. An introduction to biofluid mechanics-basic models and applications, *Journal of Biomechanics* 2002; 35(4): 415–435.
8. Ismail, A., Ademola, B. L., Yusuf, L., Abdulmalik, M. A. Renal arterial Doppler velocimetric indices among healthy subjects in north west Nigeria. *Journal of West African College Surgery* 2018; 8(1): 40-49.
9. Okoye, I. J., Agwu, K. K., Idigo, F. U. Normal sonographic renal length in adult southeast Nigerians. *African Journal of Medical Sciences* 2005; 34(2): 129-131.
10. Maaji, S. M., Daniel, O., Adamu, B. Sonographic measurement of renal dimensions of adults in North-western Nigeria: a preliminary report. *Sub-Saharan Afr J Med*, 2015; 2: 123-127.
11. Leonardo, S., and Simeone, A. Doppler ultrasound in kidney diseases: a key parameter in clinical long-term follow-up. *Journal of Ultrasound* 2016; 19(4): 243-250.

ISSN No. 2454-6194 | DOI: 10.51584/IJRIAS | Volume VIII Issue IV April 2023

12. Leoncini, V, G., Derchi, L, E., Pontremoli, R. Ultrasound Doppler renal resistive index: a useful tool for the management of the hypertensive patient Francesca. *Journal of Hypertension*, 2014; 32: 149-153.
13. Von Reutern., G. and Von Budingen., H. Ultrasound Diagnosis of Cerebrovascular Disease: Doppler sonography of the extra- and intracranial arteries duplex scanning. Stuttgart : Thieme, Barcelona, Spain 1994; 46:
14. Yoneyama., K. Saito., K. Sugihara., H. Ultrasound diagnosis of cerebral vascular disease-supplementary presentation with special reference to intracranial vessels. *Rinsho Shinkeigaku* 1995; 35(12):1585-1587.
15. Qinghui., Z. Yufeng., Z. Yi., Z. Kun., Z. Kexin., Z. Lian., G. An Ultrasound Simulation Model for the Pulsatile Blood Flow Modulated by the Motion of Stenosed Vessel Wall. *BioMed Research International* 2016; 16: 1–16.
16. Schlaikjer., M. Torp-Pedersen., S. and Jensen., J. A. Simulation of RF data with tissue motion for optimizing stationary echo cancelling filters, *Ultrasonics* 2003; 41(6): 415-419.
17. Hoogstraten., H. W. Kootstra., J. G. Hillen., B. Krijger., J. K. B. and Wensing., P. J. W. Numerical simulation of blood flow in an artery with two successive bends. *Journal of Biomechanics* 1996; 29(8):1075-1083.
18. Oung., H. and Forsberg., F. Doppler ultrasound simulation model for pulsatile flow with non axial components. *Ultrasonic Imaging* 1996; 18(3): 157-172.
19. Botnar., R. Rappitsch., G. Scheidegger., M. B. Liepsch., D. Perktold., K and Boesiger., P. Hemodynamics in the carotid artery bifurcation: a comparison between numerical simulations and in vitro MRI measurements. *Journal of Biomechanics* 2000; 33(2): 137-144.
20. Buriev., B. Kim., T. and Seo., T. Fluid-structure interactions of physiological flow in stenosed artery. *Korea Australia Rheology Journal* 2009; 21(1): 39-46.
21. Tang., D. Yang., C. Walker., H. Kobayashi., S. and Ku., D.N. Simulating cyclic artery compression using a 3D unsteady model with fluid-structure interactions. *Computers and Structures*, 2002; 80 (21): 1651-1665.
22. Tang., D. Yang., C. Kobayashi., S. Zheng., J. and Vito., R.P. Effect of stenosis asymmetry on blood flow and artery compression : a three-dimensional fluid-structure interaction model. *Annals of Biomedical Engineering* 2003; 31(10): 1182-1193.
23. Belzacq., T. Avril., S. Leriche., E. and Delache., A. A numerical parametric study of the mechanical action of pulsatile blood flow onto axisymmetric stenosed arteries. *Medical Engineering and Physics* 2012; 34 (10): 1483-1495.
24. Liand., Z. Kleinstreuer., C. Blood flow and structure interactions in a stented abdominal aortic aneurysm model. *Medical Engineering and Physics*, 2005; 27(5): 369-382.
25. Valencia and F. Baeza, "Numerical simulation of fluid– structure interaction in stenotic arteries considering two layer non linear anisotropic structural model. International Communications in Heat and Mass Transfer 2009; 6(2): 137-142, 2009.
26. Valencia., A. and Villanueva., M. Unsteady flow and mass transfer in models of stenotic arteries considering fluid-structure interaction. *International Communications in Heat and Mass Transfer* 2006; 33(8): 966-975.
27. Schlaikjer., M. Torp-Pedersen., S and Jensen., J.A. Simulation of RF data with tissue motion for optimizing stationary echo cancelling filters. *Ultrasonics* 2003; 41(6): 415-419.
28. Schlaikjer., M. Petersen., S.T. Jensen., J.A. and Stetson., P.F. Tissue motion in blood velocity estimation and its simulation. *Proceedings of the International Ultrasonics Symposium* 1998; 1495-1500.
29. Swillens., A. Løvstakken., L. Kips., J. Torp., H. and Segers., P. Ultrasound simulation of complex flow velocity fields based on computational fluid dynamics, *IEEE Transactions on Ultrasonics, Ferroelectrics, and Frequency Control* 2009; 56(3): 546-556
30. Swillens., A. Degroote., J. Vierendeels., J. Lovstakken., L. and Segers., P. A. Simulation environment for validating ultrasonic blood flow and vessel wall imaging based on fluid-structure interaction simulations: ultrasonic assessment of arterial distension and wall shear rate. *Medical Physics* 2010; 37(8): 4318–4330.
31. Swillens., A. De Schryver., T. Løvstakken., L. Torp., H. and Segers., P. Assessment of numerical simulation strategies for ultrasonic colour blood flow imaging, based on a computer and experimental model of the carotid artery. *Annals of Biomedical Engineering*, 2009; 37(11): 2188-2199.
32. Balocco., S. Basset., O. Azencot., J. Tortoli., P. and Cachard., C. 3D dynamic model of healthy and pathologic arteries for ultrasound technique evaluation. *Medical Physics* 2008; 35(12): 5440-5450.
33. Swillens., A. Segers., P. and Lovstakken., L. Two-dimensional flow imaging in the carotid bifurcation using a combined speckle tracking and phase-shift estimator: a study based on ultrasound simulations and in vivo analysis," Ultrasound in Medicine and Biology 2010; 36(10): 1722-1735.

ISSN No. 2454-6194 | DOI: 10.51584/IJRIAS | Volume VIII Issue IV April 2023

34. Apelt, K., Bijkerk, R., Lebrin F., Rabelink, T. J. Imaging the Renal Microcirculation in Cell Therapy. Cells 2021, 10, 1087. https://doi.org/10.3390/cells10051087
35. Hernandez, G. E., & Leduc, J. A. V. The Correlation Between Interlobar Artery Diameter and the Systolic Pressure of Pulmonary Artery in the Diagnosis of Pulmonary Hypertension. *Chest*, 2011, 140(4):709A. doi:10.1378/chest.1119484
36. Sharma A, et al. (2018) Modulation of the Formation of Aβ- and Sup35NM-Based Amyloids by Complex Interplay of Specific and Nonspecific Ion Effects. *J Phys Chem B* 122(19):4972-4981
37. Olowoyeye, O. A., Gar-Wai Chiu, S. E., Wright, G. A. and Moody, A. R. Analysis of the Velocity Profile of the Popliteal Artery and Its Relevance During Blood Flow Studies, *Journal of Diagnostic Medical Sonography* Volume 33 (6): 489-497, November/December 2017.
38. Shiva Manjunath R. G. and Rana, A. Nanotechnology in Periodontal Management, 2015, 6(1): 1 – 8